Typeset using LaTeX default style in AASTeX631

The effect of the Io plasma torus on precise orbit determination and gravity recovery. Application to Europa Clipper.

Gael Cascioli [1,2] Erwan Mazarico [2] Flavio Petricca [3] Andrea Magnanini [4] Dustin R. Buccino [3] Martina Ciambellini [5] Antonio Genova [5] Luis Gomez Casajus [4] Marco Zannoni [4] and Paolo Tortora [4]

[1] University of Maryland Baltimore County, 1000 Hilltop Circle, Baltimore, MD 21250, USA
[2] NASA Goddard Space Flight Center, 8800 Greenbelt Road, Greenbelt, MD 20771, USA
[3] NASA Jet Propulsion Laboratory, California Institute of Technology, 4800 Oak Grove Dr, Pasadena, CA 91011, USA
[4] Alma Mater Studiorum —Università di Bologna Via Fontanelle, 40, 47121, Forlí, Italy
[5] Università La Sapienza, Via Eudossiana 18, Rome, 00184, Italy

ABSTRACT

The neutral gases released by the intense volcanic activity of the Jupiter moon Io, once ionized by the Jupiter magnetic environment, give rise to a toroidal plasma distribution known as Io Plasma Torus (IPT). Radio signals passing through charged particles environments, such as the IPT, are heavily perturbed, proportionally to the rate of change of the charged particle distribution along the path of the radio wave. If not properly calibrated, the IPT may induce significant perturbation on the radiometric tracking link to Earth. The radio tracking signal is the main observable for the Gravity and Radio Science (G/RS) investigation on NASA's Europa Clipper whose aim is to measure the gravity field, tidal response and moment of inertia of Europa, and to precisely reconstruct the trajectory of the probe in support to other scientific investigations. In this work we quantify the detrimental effect of the IPT on the radiometric observables. We show how this affects the products of the G/RS and prove the necessity for accurate calibrations. We simulate different calibration strategies to mitigate its perturbative effect, based on currently available models of the IPT. Considering that these models have been developed with Juno in mind, they are tailored to its orbital geometry and we show that they cannot be easily applied to other geometries. We conclude that although the model-based calibration strategies can be very effective, further work will be needed to make them applicable to probes with a significantly different orbital geometry, such as Europa Clipper or ESA's JUICE.

1. INTRODUCTION

Before the Voyager flyby of the Jupiter system, ground-based observations led to the detection of a toroidal-shaped distribution of ionized sulfur whose nature was poorly understood (Kupo et al. 1976). By the time in-situ measurements were collected by the Plasma Science instrument onboard Voyager 1 and provided a first characterization of the plasma environment (Bridge et al. 1979; Eshleman et al. 1979), it was clear that the main source of this plasma distribution was the intense volcanic activity of Io (*e.g.,* Peale et al. 1979). Io ejects neutral gas at a rate of about 1 ton/s (Bagenal & Delamere 2011), which is then ionized by electron collisions and results in a toroidal distribution of plasma called Io Plasma Torus (IPT), subject to electromagnetic, gravitational and centrifugal forces. The plasma achieves a configuration of minimum centrifugal potential at the centrifugal equator. The torus which on this plane, has its peak density at a distance equal to Io's orbital distance from Jupiter ($5.9\,R_J$, where $R_J = 71492\,km$ is Jupiter's equatorial radius). Data from Voyager 1 were extensively used to build spatially-varying models of the distribution of these charged particles, which helped understanding that the IPT is divided into three regions distinguished by their mean plasma temperature, charged particle density, and radial extension (*e.g.,* Bagenal et al. 1980; Bagenal 1994a). The innermost region is called the cold torus because of the low plasma temperature and charged particles density (~ 1000 cm^{-3}). It is surrounded by a narrow region called the ribbon, where the density is higher (~ 3000 cm^{-3}). Finally, the outermost region, the warm torus, is characterized by an intermediate density (~ 2000 cm^{-3}). Plasma measurements acquired by Galileo (Bagenal et al. 1997) were used to refine these models, which were used as reference until the arrival of Juno in the Jupiter system (Phipps & Withers 2017).

While earlier models of the IPT were based only on data from ultraviolet spectrometers and plasma instruments, NASA's Juno provided an additional tool for sounding the plasma distribution, based on the radiometric Doppler tracking data collected by the Gravity Science experiment (Asmar et al. 2017) (only two other radiometric measurements had been obtained prior to Juno, one from Voyager 1 and one from Ulysses (Eshleman et al. 1979; Bird et al. 1992)). Because the perturbations affecting the radiometric signals propagating through a plasma are frequency-dependent , probing the IPT with simultaneous measurements at multiple frequencies can reveal the electron density distribution (Phipps & Withers 2017). This capability was enabled by the radiofrequency system used for Juno's Gravity Science experiment that allowed to simultaneously acquire coherent radiometric data at X-band (7.2 - 8.4 GHz) and Ka-band (32.1 GHz - 34.0 GHz) (Asmar et al. 2017). Data around Juno perijoves were obtained and used in different subsequent solutions to refine IPT electron density modeling (Phipps et al. 2018, 2019, 2021; Moirano et al. 2021).

As such, the strong effects of plasma on the Doppler data present an opportunity to study and characterize the IPT. On the other hand, the IPT effects, if uncalibrated, may introduce significant undesired perturbations on the same tracking data during the gravity science experiment analysis . When multi-frequency radiometric data are available , the plasma effects can be calibrated out by combining the different frequencies and leveraging their differential sensitivity to the plasma (Bertotti et al. 1993). However, gravity and radio science investigations based on a single-frequency link cannot employ this self-consistent calibrations strategy, potentially leading to a degradation of the gravity results. In a recent reanalysis of the radio science data acquired at Europa by Galileo, Gomez Casajus et al. (2021) showed that the IPT likely introduced strong perturbations in the measurements collected during the flyby E26. The E26 data had to be disregarded in order to prevent biases in the gravity solution. The failure that affected Galileo's high-gain antenna (HGA) only allowed the acquisition of radiometric data at lower frequency (S-band, 2.3 GHz), which are more impacted by the detrimental effects of plasma, but even X-band data can be expected to be significantly affected.

The Europa Clipper Gravity/Radio Science (G/RS) investigation will study the interior structure of Europa through measurements of its gravity field obtained with X-band radiometric data (Mazarico et al. 2023). The use of a single-frequency link for establishing Doppler tracking makes the Europa Clipper experiment particularly sensitive to the effect of the IPT. A thorough assessment of the expected perturbation and a survey of possible calibration strategies is thus necessary. In this paper, we focus on the Europa Clipper G/RS investigation. We aim to quantify the potential effects of the IPT on the Precise Orbit Determination (POD) and on the recovery of Europa's static gravity field and tidal response. Based on the knowledge of the IPT derived from Juno data, we model the distribution of the plasma in the IPT and quantify the perturbation on the Doppler data that will be acquired by Europa Clipper during the flybys of Europa. We simulate the G/RS investigation using multiple models of the IPT produced by different authors (*e.g.,* Phipps et al. 2018; Moirano et al. 2021), and assess the effects of uncalibrated plasma perturbations on the reconstruction of the spacecraft trajectory and gravity field of Europa. Subsequently, we evaluate the effectiveness of model-based calibrations of the plasma effects. Because of the significantly different orbital geometries involved, we show that the applicability of models elaborated with Juno data to Europa Clipper's data is not straightforward. Finally we discuss our findings, suggesting the necessity of an improved knowledge of the IPT, and propose reasonable strategies to achieve this.

This manuscript is structured as follows: we first provide the theoretical basis for the computation of the IPT-induced perturbation (Sec. 2) and review the available models of the IPT charged particle density, highlighting their limitations and the complications involved in their application to Europa Clipper (Sec. 2.1). Then, in Section 3 we describe model-based calibration techniques. We investigate in detail the case of Europa Clipper (Sec. 4) by first analyzing the net perturbative effect of the IPT (Sec. 4.1) on the gravity field and trajectory reconstruction products of the G/RS, then by exploring the effectiveness of model-based calibration strategies (Sec. 4.2), and quantify the effect of IPT model parameters uncertainty (Sec. 4.3). We also provide an assessment of the IPT effect on the reconstruction of Europa's ephemerides in Section 4.4. Finally we discuss the results and propose a path forward for ameliorating currently available IPT models (Sec. 5) and provide our conclusions in Section 6.

2. IPT EFFECT ON RADIOMETRIC TRACKING

Deep space spacecraft trajectories are reconstructed using Precise Orbit Determination (POD). In a nutshell, the ground station transmits a radio wave of known frequency which is received and transponded back by the spacecraft. The motion of the spacecraft (which depends on the physical environment it is flying in) induces a Doppler shift, which is the main observable quantity in POD. POD consists in finding the parameters of the model describing the spacecraft

motion that allow to best fit the observed Doppler signal (the interested reader is referred to, *e.g.,* Tapley et al. 2004; Milani & Gronchi 2009, for further details. See also Appendix A). For the solution of POD to be reliable and accurate all sources of Doppler shift higher than the measurement system noise floor must be accurately modeled. Typical examples of these Doppler-shift generating sources are: the gravity field of the celestial bodies in close proximity of the spacecraft, the solar radiation pressure acceleration, the radiative accelerations (e.g., thermal infrared pressure, albedo pressure, etc), and media effects due to *e.g.,* Earth ionosphere and interplanetary plasma. The IPT is another source of Doppler shift. The presence of the IPT along the radio wave propagation path has the effect of changing the refractive index of the medium. A variation of the refractive index n induces a variation in the propagation speed of the radio wave, or equivalently a variation of the signal optical path Δl. The variation in time of Δl generates a Doppler shift. The fractional frequency shift $y(t)$ is given by:

$$y(t) = \frac{f(t) - f_0(t)}{f_0(t)} = \frac{1}{c}\frac{d\Delta l}{dt} \tag{1}$$

where $f(t)$ is the received frequency at the ground station at time t, $f_0(t)$ is the reference frequency (i.e., the frequency that was transmitted by the ground station) and c is the speed of light. It can be shown that for an ionized medium (*e.g.,* Bertotti et al. 1993):

$$\Delta l = \int (n(s) - 1)ds = -\int \frac{e^2}{2\pi m_e f_0^2} n_e(s) ds \tag{2}$$

where m_e, e are the electron mass and charge, respectively, n_e is the electron density of the medium and the integration is performed the effective radio propagation path defined by the line coordinate s. It follows that radio waves received and re-transmitted by a moving spacecraft in the Jovian environment may be subject to a significant Doppler shift induced by the IPT when the radio wave crosses its regions of strongly spatially-variable electron density. This signal needs to be accurately calibrated in order to obtain reliable POD results. As described by Equation 2, this is a dispersive effect, *i.e.,* it is frequency dependent. As shown in Bertotti et al. (1993) the use of multi-frequency links (*i.e.,* multiple simultaneous links at different frequencies in uplink and/or downlink) enables to single out the non dispersive contributions and use these measurements for a complete calibration of the dispersive effects. This calibration scheme has been extensively used for removing solar plasma in the radio tracking datasets of Cassini (*e.g.,* Bertotti et al. 2003) and BepiColombo (*e.g.,* Cappuccio et al. 2020) and to remove both the IPT and solar plasma contributions in the Juno dataset (*e.g.,* Durante et al. 2020). Most notably the dispersive calibrations obtained by Juno have been used to refine and update the models describing the morphology and dynamics of the IPT (Moirano et al. 2021; Phipps et al. 2018, 2021).
In a single-link configuration, as is the case for Europa Clipper, this calibration strategy cannot be employed, and physical models describing the electron density of the IPT are needed in order to compute its effect on the radiometric observable and therefore remove it from the dataset.

2.1. *Models of Io Plasma Torus electron density*

In this work we make use of two sets of models, notably the ones derived by Phipps et al. (2018, 2021), from now on referred to as *Phipps+18*, and the ones derived by Moirano et al. (2021), from now on referred to as *Moirano+21*. Both models are derived from the semi-empirical formulation developed by Bagenal & Sullivan (1981) and Bagenal et al. (2017) based on Voyager data, and updated with Juno observations. Both Phipps+18 and Moirano+21 models describe the electron density field n_e in a centrifugal reference frame co-aligned with the IPT. Figure 1 shows a representation of these main density models. The model introduced by Moirano et al. (2021) is based on the same formulation as Phipps et al. (2018), further modified to be tailored to the orbital geometry of Juno. Notably, the authors recognized that the majority of the variation in the total electron content (TEC) in Juno's observation is due to vertical crossing of the IPT plane (*i.e.,* the Juno radio waves are nearly parallel to the IPT plane and as Juno moves along its polar orbit the radio wave probes different off-plane regions of the IPT always crossing it in one location and in a direction that is substantially radial from Jupiter, see Figure 2). This led the authors to change the base model and use a single region to model the ribbon, the warm, and the extended torus as Juno data is not sensitive to any of the region individually but rather to their sum.

The other main difference between the two sets of models consists in their longitudinal and temporal dependency. While Phipps et al. (2021) found a longitudinal dependence of the TEC measured by Juno, this is not explicitly

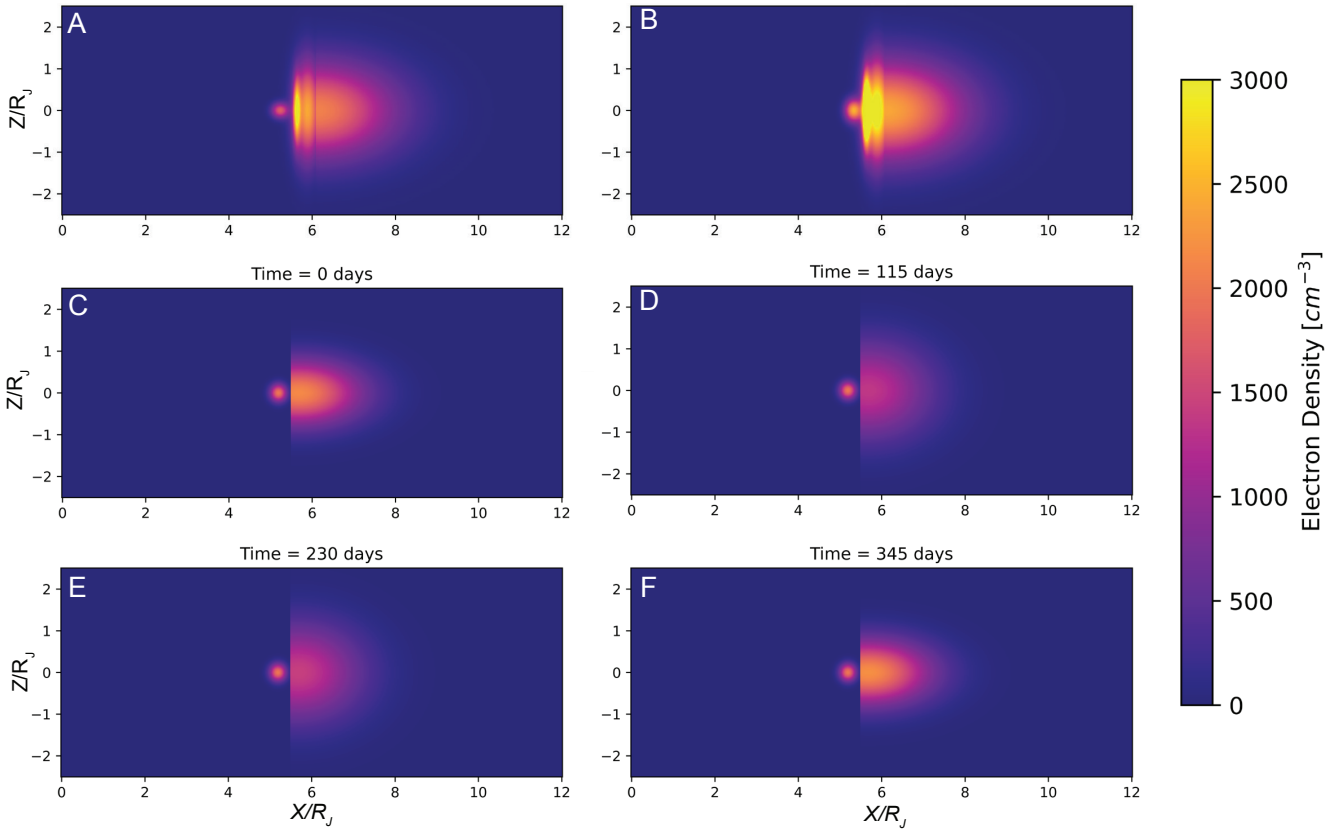

Figure 1: Electron density distribution given by different models. Panels A and B show the Phipps B and Phipps G models respectively (Phipps et al. 2018). Panels C, D, E and F show four time snapshots of the Moirano model (Moirano et al. 2021). The horizontal and vertical axes of all panels correspond to the x and z axes of the IPT centrifugal reference frame normalized by Jupiter radius R_J. All panels show a vertical slice of the electron density field at centrifugal longitude $\lambda = 0$

factored in the density model. As a result Phipps et al. (2021) provided revised values of the model's coefficients, showing that slightly different values are needed to fit different Juno flybys, possibly because of temporal-longitudinal variability. The two main models they developed are called Model B and Model G. These have different equatorial tilts to account for the observed data. Model G, with a tilt of 7.7° fits better Juno PJ1 and is compatible with the Ulysses and Voyager observations (Bird et al. 1993).

The Moirano+21 model does instead explicitly account for temporal and longitudinal variations. This allowed the authors to perform fitting of the model parameters over 15 Juno perijoves simultaneously and the estimation of both the central value and the 1-sigma confidence interval for each parameter of the model .

Figure 1 shows a cross-section of the electron density field of the IPT for three different models. Although both models sets are , the electron density values are noticeably different.

As can be observed in Figure 1, both sets of models contain at least one discontinuity in the electron density profile (or more precisely: the density profiles are not continuously differentiable). This discontinuity happens at $R = 6.1R_J$ for Phipps+18 models and at $R = 5.5R_J$ for the Moirano+21 model. This is a direct consequence of the specific analytical representation that has been chosen for n_e, *i.e.,* a piece-wise composition of Gaussian functions. The orbital and tracking geometry of Europa Clipper (and Jupiter-system investigation probes like ESA's JUICE) is substantially different from Juno. Not only does the radio path generally cross the IPT twice, as opposed to once for Juno, on its way to Earth, but it also crosses the IPT in varied geometries, not only radially outwards like Juno.

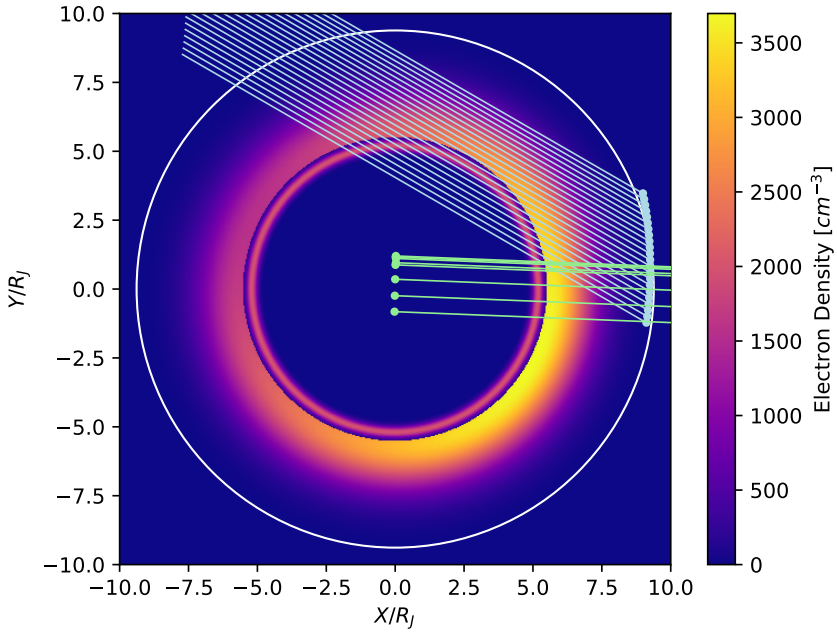

Figure 2: Comparison of the radio beam path in the case of Juno (green lines) and Europa Clipper (light blue lines). In the background the electron density computed from Moirano+21 is shown to highlight that in certain geometries the radio beam of Europa Clipper might cross the discontinuity of the model (thin dark ring at $\sim 5R_J$), producing spurious spikes in the IPT Doppler perturbation computed from the model (see also Figure 3a). Horizontal and vertical axes denote the distance from Jupiter normalized by the Jupiter radius R_J. The white circle shows the orbit of Europa. All the quantities are drawn in an inertial reference frame aligned with the centrifugal equator.

The discontinuity present in the models has a significant impact on the computed Doppler perturbation (proportional to the time derivative of n_e) when the signal crosses the torus (and the density 'gap') in a direction nearly tangential to the torus itself, a condition relatively frequent for Europa Clipper. This aspect is exemplified in Figure 2 where we represent the Juno signal path geometry during a perijove, and the geometry of the radio path during one Europa Clipper flyby.

This geometrical configuration leads to stark discontinuities in the model-computed differential density and the discontinuity in the model reflects on the computed Doppler perturbation by generating spurious peaks (Figure 3a). Notably, these peaks occur at different times consistently with the two sets of models having discontinuities at different distances from Jupiter. It is important to underline that this phenomenon does not affect the Juno geometries, as the signal path never crosses the discontinuity tangentially.

To overcome this limitation of the currently available models we slightly modify their analytical definition by introducing a non-linear taper (see details in Appendix B) between segments of the model that do not connect with continuity. Figure 4 shows a comparison of a radial electron density profile computed using the original and tapered models and Figure 3b shows the corresponding Doppler perturbations which now do not show spurious peaks. In the following we will always use the tapered models, and we will refer to them as Phipps+18t and Moirano+21t.

3. MODEL-BASED CALIBRATION TECHNIQUES

The end goal of this work is to quantify the effect of the IPT on the Gravity and Radio Science (G/RS) experiment of Europa Clipper (Mazarico et al. 2023). G/RS relies on the precise OD of the spacecraft. As discussed in Section 2, the in-depth modeling of all error and noise sources in the radiometric observables used for OD is of paramount importance to obtain a reliable estimate of the key geophysical parameters constituting the scientific objectives of G/RS. For this reason, a calibration technique for mitigating the effects of the IPT perturbation on the Doppler link between the probe and the ground station has to be devised. The simplest calibration technique consists in using the

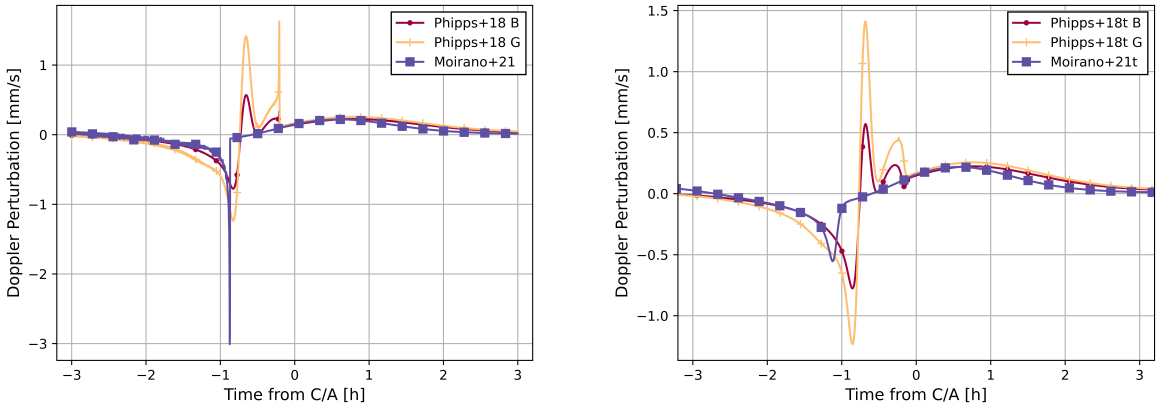

(a) Doppler perturbation from the original models

(b) Doppler perturbation from the tapered models

Figure 3: Doppler perturbation computed from different IPT models for one Europa Clipper flyby (shown in Figure 2). The abrupt peaks visible in the signals in the left panel are due to discontinuities in the underlying models. The right panel shows the signal computed on the same flyby with the models modified using the non-linear taper (see Appendix B). It can be clearly seen that the spurious peaks have been mitigated.

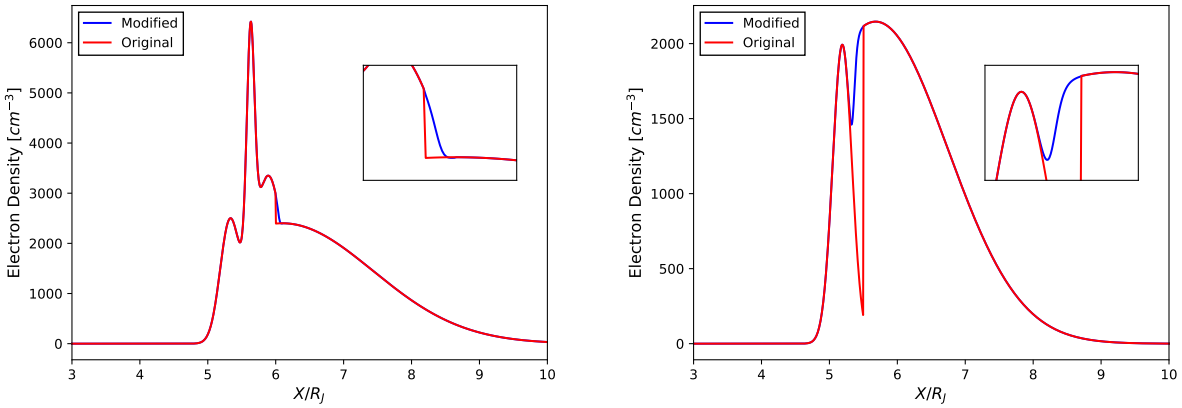

(a) Phipps+18 G model

(b) Moirano+21 model

Figure 4: Radial electron density profiles obtained with two different models when applying a non-linear taper to remove the discontinuities in the models (See Appendix B).

available models of the IPT electron density to compute the perturbation. From the previous discussion we know that the available IPT models show differences among each other because of model assumptions and data-reduction assumptions (*e.g.,* Phipps+18 B and Phipps+18 G) or show an intrinsic uncertainty of their constitutive parameters (Moirano+21). For this reason we cannot simply assume a model to be perfectly capturing the perturbative effect of the IPT, but rather we have to take into account the possibility that after applying the model-based calibration a residual effect remains. Thus in the following we will test different cases to quantify these effects. Namely we will assume that the *true* perturbation (*i.e.,* the one used to simulate the tracking data) is due to the Phipps+21t B model, while the *model* perturbation (*i.e.,* the one used in the OD process) is either Phipps+18t G or one or more realizations of the Moirano+21t model (varying the model parameters within the stated uncertainty). These two sets of cases allow us to explore the range of expected results in a realistic scenario where we cannot assume to know the exact behavior of the IPT.

More sophisticated techniques could be devised, but are likely not applicable to the Europa Clipper case. For example,

one mitigation strategy could involve the techniques that allow for data-based model scaling and data-model assimilation. The first class of methods consists in correcting the tracking data with the calibration computed from one of the models, and in the process estimating from the data a factor to scale the computed model calibration (similarly to what is sometimes done for the tropospheric and ionospheric effects of planetary atmospheres *e.g.,* Cascioli et al. (2020)). Arguably, however, this class of methods cannot be applied to the Europa Clipper case. Because of the flyby geometry, the maximum of the IPT perturbation normally occurs the closest approach, *i.e.,* when the radio beam crosses the orbital plane of Europa . Data acquired at the closest approach are the most sensitive to the body gravity field, thus estimating scale factors capable of absorbing the IPT perturbation will likely result in capturing the information associated with the unknown gravity signal at the closest approach, attributing it to the IPT rather than to the actual subsurface density distribution. The second class of methods (data-model assimilation) are techniques allowing to estimate the key parameters of the IPT model and feed them back into the model for the radiometric signal calibration. For these techniques to be applicable, the radiometric signal needs to be independently sensitive to the IPT perturbation, for example using dual-frequency links, which is not applicable to Europa Clipper G/RS that will employ a single X-band ($\sim$ 8 GHz) link. Another possibility consists in de-weighting the tracking data that are expected (based on the IPT model) to be heavily affected by the IPT perturbation, such that they have a smaller influence on the OD solution. For the same reasons stated above (the maximum perturbation often occurs at the closest approach), this is not an optimal solution, as it would reduce the overall sensitivity to the gravity field of Europa.

4. APPLICATION TO EUROPA CLIPPER

In the following we want to quantify the effects of the IPT on the orbit and gravity field reconstruction that can be performed by Europa Clipper. To this aim, we first assess the influence of the IPT on the Europa Clipper investigations, by simulating its POD using the latest tour trajectory and G/RS investigation assumptions. . After quantifying the net effect of the IPT, in the case no calibration technique is applied, we will quantify the beneficial effect of the simple calibration techniques discussed in the previous paragraph. We simulate the POD process, core to the G/RS experiment, using the same detailed simulation scenario employed in previous works (Mazarico et al. 2023; Cascioli et al. 2024). This includes realistic assumptions for tracking link noise, the latest nominal trajectory of the Jovian tour (21F31V7), a realistic tracking scenario (scheduling of spacecraft and Earth antennas). In the OD process, considering $\pm$2 hours around the closest approach, we solve for the trajectory of the spacecraft and a scale factor for the solar radiation pressure, alongside the key geophysical parameters of interest to the G/RS experiment. These include the static gravity field of Europa (GM and spherical harmonics coefficients up to degree and order 15), the tidal response of the moon (parameterized by the Love number k_2), the orientation of Europa (spin axis orientation, spin rate and libration amplitude). Figure 5 provides an overview of the influence of the IPT during the $\pm$ 2 h tracking windows of the 49 flybys that will be performed by the probe. Notably we show the RMS perturbation on the Doppler signal, computed from the different models, when the spacecraft is closer than 10,000 km to the surface of Europa (to limit the analysis to the portions of the trajectory that are most sensitive to the gravity field of Europa, hence most important for trajectory reconstruction, parameters estimation, and the geolocation of the high-resolution data collected by the other instruments onboard Europa Clipper).

Given the tour design, it is clear that the second half of the flybys will be the most affected by the IPT (from now on we refer to the first part of the Europa Campaign as EC1, up to and including flyby 29. We refer to the second part as EC2). This implies also that the IPT perturbation mostly impacts flybys occurring on the sub-jovian hemisphere of Europa, while the coverage on the anti-jovian hemisphere is substantially unaffected (see Figure 16 in Appendix D and Fig. 19 in Mazarico et al. (2023)). Moreover Figure 5 highlights the high variability between different models (Phipps+18 B, Phipps+18 G and Moirano+21) and the variability within a single model (Moirano+21 (sample)). This latter case simply indicates a different realization of the Moirano et al. (2021) model, meaning that the model parameter values are drawn from a normal distribution with the same mean and standard deviation obtained by the authors. The two sets of models, moreover show a large discrepancy during the first half of the tour, when the Europa Clipper-to-Earth geometry is more favorable in terms of IPT perturbation, *i.e.,* when the radio beam does not cross the peak electron density, but rather remains in the external regions. This is well explained by the different spatial decay of the two different sets of models (see Figure 1).

We can thus anticipate that the IPT will mainly affect the POD results obtained with data from the second portion of the tour. The simplest solution for limiting the IPT detrimental effect would consist in limiting the POD solution

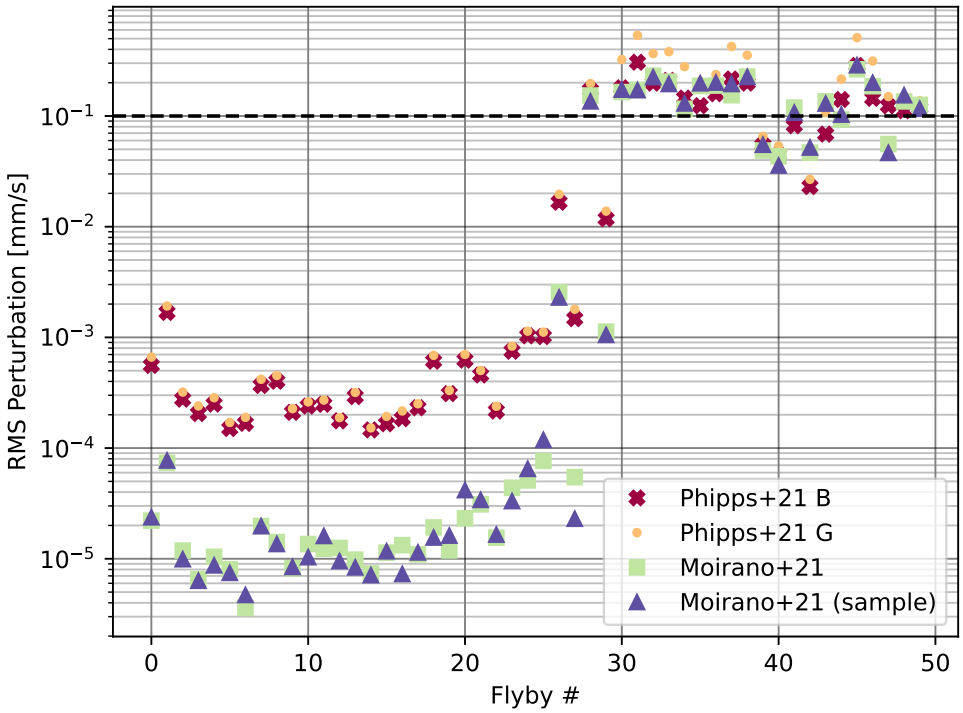

Figure 5: RMS perturbation of the IPT on the 2-way Doppler tracking signal of Europa Clipper. The RMS perturbation is computed only on the tracking data collected 10000 km from the surface and lower. Different markers indicate different IPT electron density models. Namely Phipps+18 B and G refer to the B and G models in Phipps et al. (2018, 2021), Moirano+22 refers to the model defined by Moirano et al. (2021) using its central values, while Moirano+22 (sample) indicates the same model, but with model parameter values drawn from a normal distribution compatible with the uncertainty of the parameters reported in the manuscript. The horizontal line shows the approximate value of the expected data noise of Europa Clipper ($\sim 0.1 mm\, s^{-1}$). All the models considered here have been smoothed with a non-linear *taper* (hence the name suffix "t", see Sec. 2.1 and Appendix B)

to only EC1. The Europa Clipper tour has been built to ensure the robustness of the main science requirements (Pappalardo et al. 2024). For G/RS the only science requirement consists in the retrieval of the tidal Love number k_2 with an uncertainty lower than 0.06 (Mazarico et al. 2023). In addition to the one formal science requirement, G/RS aims to deliver many more foundational results for the understanding of Europa. Notably, as discussed in detail in Mazarico et al. (2023), G/RS will enable measuring the moment of inertia factor (MOIF) of Europa to up to a factor of 15 better than previous estimates and determining whether Europa is in hydrostatic equilibrium (through the ratio between J_2 and C_{22}) with an uncertainty of a factor of better than what is currently available. Another important parameter that G/RS will is the mass of the body (through its gravitational constant GM).
Figure 6 shows the evolution of uncertainty with the inclusion of each flyby data. We normalize the uncertainty of each parameter to the value that could be obtained with the analysis of the full dataset (see the actual values in Table 1). Using only EC1 data leads to an acceptable uncertainty for the k_2 solution (since its retrieved uncertainty would increase only by a factor of ~ 1.6, still below the target accuracy) confirming the robustness of the tour design. However, many of the other key parameters that G/RS can measure would see a much degraded solution. Most notably, Figure 6 shows how fundamental EC2 is for the retrieval of the MOIF and the J_2/C_{22} hydrostatic ratio.

While we note that the main scientific objective of the G/RS investigation (*i.e.,* k_2) will not be threatened by the perturbations induced by the IPT, what motivates this study is to assess the IPT detrimental impact on the other key geophysical parameters that G/RS seeks to measure, and devise and evaluate mitigation strategies to minimize it. Moreover, since several other investigations will rely on an accurate and precise trajectory reconstruction (*i.e.,* all

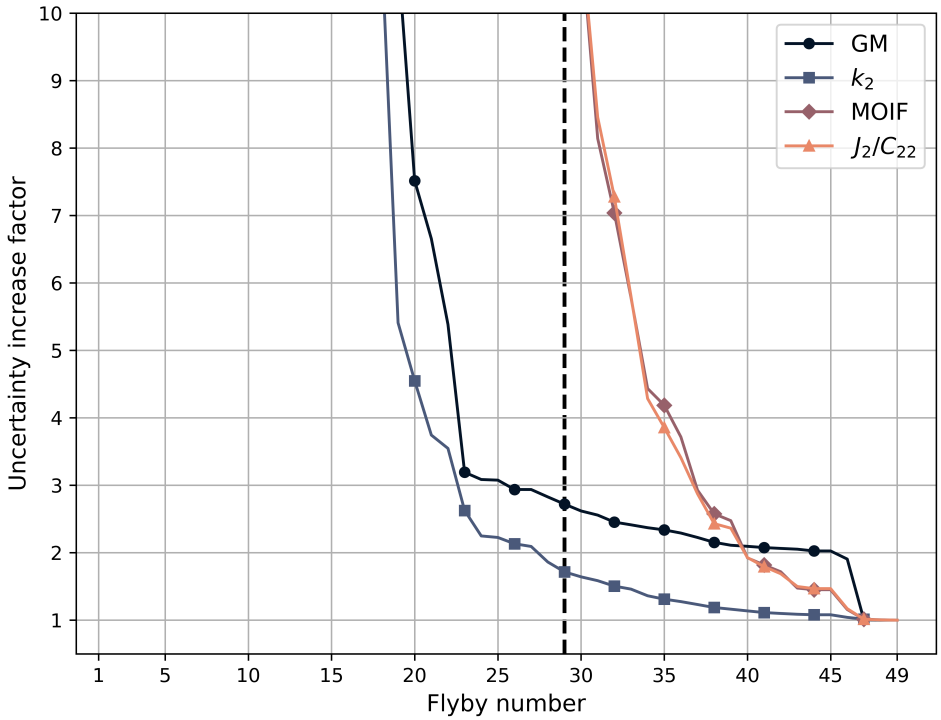

Figure 6: ncertainty evolution of key geophysical parameters measured by the G/RS investigation. The curves represent the retrieved uncertainty on the parameters as a function of the number of flybys included in the analysis. All curves are normalized to the uncertainty attainable when analyzing the whole mission (49 flybys). The vertical line denotes the transition from EC1 to EC2, when the impact of the IPT will become substantial.

investigations that need to precisely know the relative position of the spacecraft with respect to Europa) in this work we also want to assess the trajectory reconstruction performance under these adverse conditions.

4.1. *Net effect of the IPT*

First of all, we define a baseline scenario, and assess the net effect of the IPT when no calibration procedure is attempted. For this case, and for the following ones, we quantify the IPT effect on the trajectory, and on the estimation of the key geophysical parameters. The trajectory error is computed as the norm of the difference between the OD solution trajectory and the "true" trajectory (*i.e.,* the one that was used to generate the synthetic observables). For each flyby we report the RMS and the standard deviation of the total trajectory error, Figure 7.

As expected, the first half of the tour is substantially unaffected by the IPT, while in the second half of the tour the trajectory reconstruction error can reach values as high as 15 times the formal uncertainty. This is particularly exacerbated for flybys 31-38. These are low-altitude flybys (less than 50 km of altitude), whose geometry allow for continuous tracking during the closest approach, explaining why the trajectory uncertainty is significantly better (black line in Fig. 7). The magnitude difference between the different models is explained by their different amplitudes and temporal dynamics. The effect on the retrieved gravity field is of comparable amplitude. Figure 8 shows the estimation error to formal uncertainty error ratio for the retrieved gravity field spherical harmonics coefficients. The absence of calibration may lead to large errors (higher than six times the uncertainty), especially on the low degrees. This is easier to understand in a spatial representation of the gravity field. Figure 9 shows a degree 15 expansion of the gravity field resulting of the POD process. While in the fully compensated case the estimation error is well contained and statistically consistent with the retrieved uncertainty, when no calibration is applied to the IPT perturbation, the resulting gravity field is heavily biased, both at local and global scales. Figure 9 report the estimation error normalized by its associated uncertainty. We report the absolute value errors in Appendix C. Because the coverage of the leading and trailing hemispheres is less uniform than the sub- and anti-Jovian regions (see also the spatial coverage in Figure 16), the gravity anomaly uncertainty will be of the order of several tens of mGal (maximum of 40 mGals). Therefore,

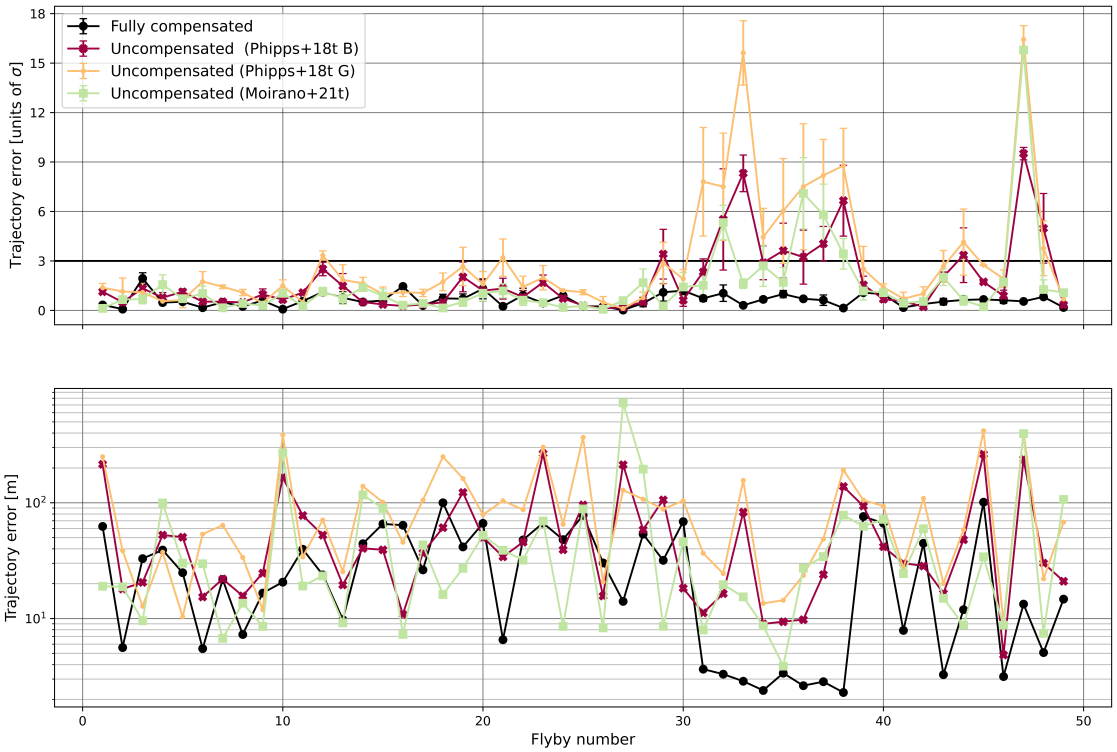

Figure 7: Trajectory error for each flyby. Both plots show the RMS trajectory error for different cases. The top panel reports the trajectory error normalized by the trajectory uncertainty (indicated by σ) together with its standard deviation (error bars), while the bottom plot shows the absolute value. The red, yellow and green lines show the error when no calibration strategy is employed, using different models to simulate the IPT behavior (Phipps+18t B, Phipps+18t G, Moirano+21t, respectively). The black line shows, for comparison, the error that one would obtain if the IPT was fully calibrated (or equivalently, there was no IPT perturbation. This is equivalent to the uncertainty in the trajectory reconstruction, which strongly depends on orbital geometry and tracking opportunities). The horizontal black line in the top panel highlights the 3σ level.

in these regions the errors in the reconstruction of the local gravity field induced by the IPT might be larger than 100 mGals.

Table 1 shows the effect on key geophysical parameters objective of the G/RS investigation, discussed in Section 4. In the table we report the error to formal uncertainty ratio. It is clear how different IPT perturbations can have a significant effect on some of these key parameters. As discussed above, because the bulk of the information on k_2 is collected during EC1 (see Figure 6), the Love number is almost insensitive to the IPT perturbation, confirming that the scientific objective of the G/RS investigation is robust. Other global geophysical parameters, conversely, may be heavily affected by uncalibrated plasma effects. GM, MOIF, and the hydrostatic ratio J_2/C_{22} show estimation errors that can reach up to more than 4σ.

4.2. *Partial calibration*

After establishing the detrimental effect that the IPT could have on the POD solution if uncompensated, we now want to assess the effectiveness of model-based corrections to aid calibrating out these perturbations. Given the variability between models, and the inherent uncertainty of the models themselves, as was well quantified in both Moirano et al. (2021) and Phipps et al. (2018), we cannot assume to know the real IPT behavior perfectly. For this reason we will first assume that the *true* IPT behavior is defined by one reference model (Phipps+18t B) and use other models for

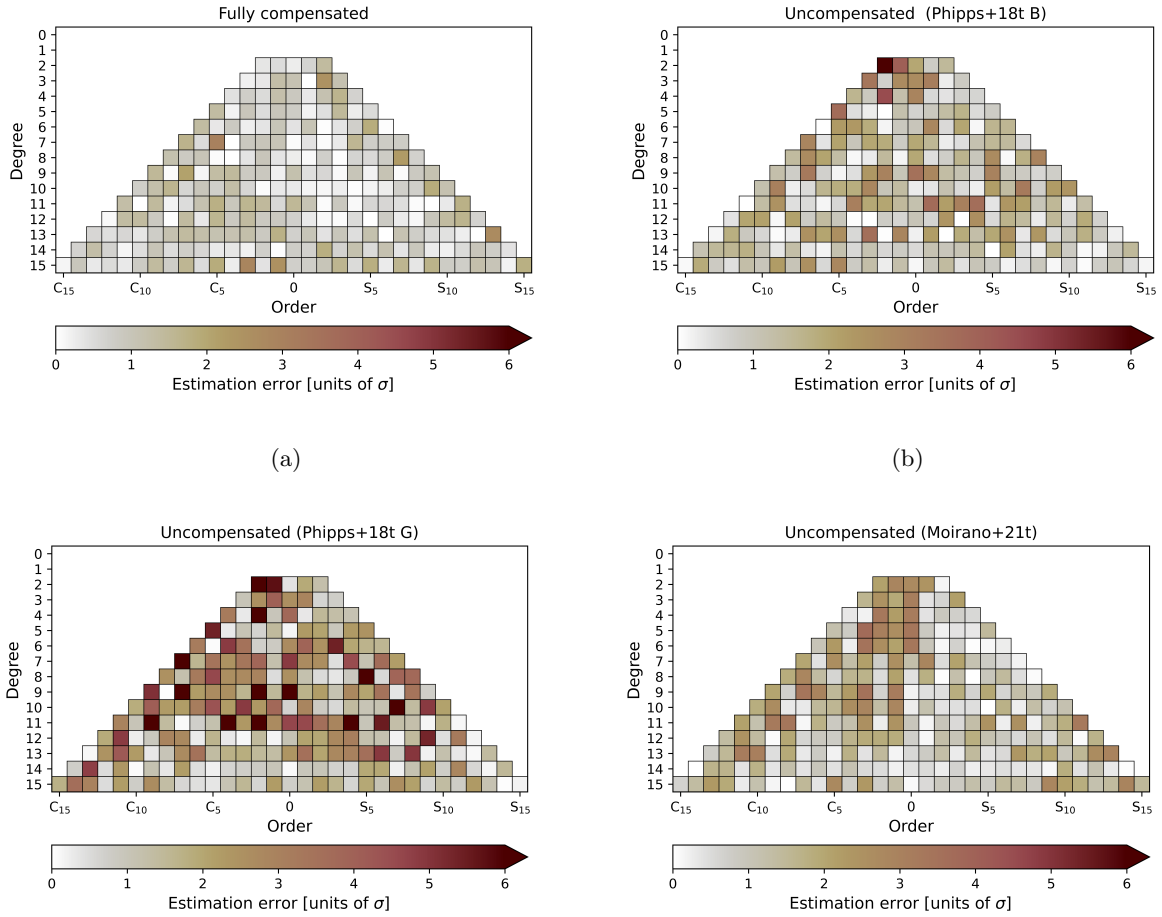

Figure 8: Gravity field spherical harmonics coefficients' reconstruction error normalized by their formal uncertainty (σ). Each panel reports the ratio between the estimation error and the formal uncertainty for all the solved-for coefficients in the classical tree-representation: vertical axis corresponds to the degree of the gravity field, horizontal axis the order (with orders on the left representing C coefficients, and S on the right). (a) reports, for comparison, the expected estimation error in the fully compensated case, (b) panel shows the same quantity when the IPT is computed from the Phipps+18 B model and no calibration technique is applied. Phipps+18t G and Moirano+21t are shown in panels (c) and (d), respectively.

computing the calibrations (Phipps+18t G and Moirano+21t). This test is aimed at quantifying the residual error introduced in the POD by a partial knowledge of the IPT structure. The results, in terms of trajectory error are shown in Figure 10. It can be clearly seen (by comparing with the uncalibrated results in Figure 7) that the partial calibration is effective in strongly reducing the average trajectory reconstruction error. Some of the flybys, however still show a significant error, above the 3σ acceptable level. Notably the Moirano+21t model performs generally worse than the Phipps+18t G model. This result is easily explained by the fact that the two sets of models are structurally different. While Phipps+18t G is structurally identical to Phipps+18t B (assumed as truth) and the only difference between the two is given by model parameters (e.g., peak amplitude), the Moirano+21t model is structurally different from the assumed *true* behavior of the IPT, so a larger error can be expected.

We also report the effect on the gravity field estimation in Figure 11. Consistently with the trajectory reconstruction, the structurally different model (Moirano+21t) leads to worse performance in the gravity field recovery, showing errors exceeding six times the associated uncertainty. The estimation error on the geophysical parameters reported in Table

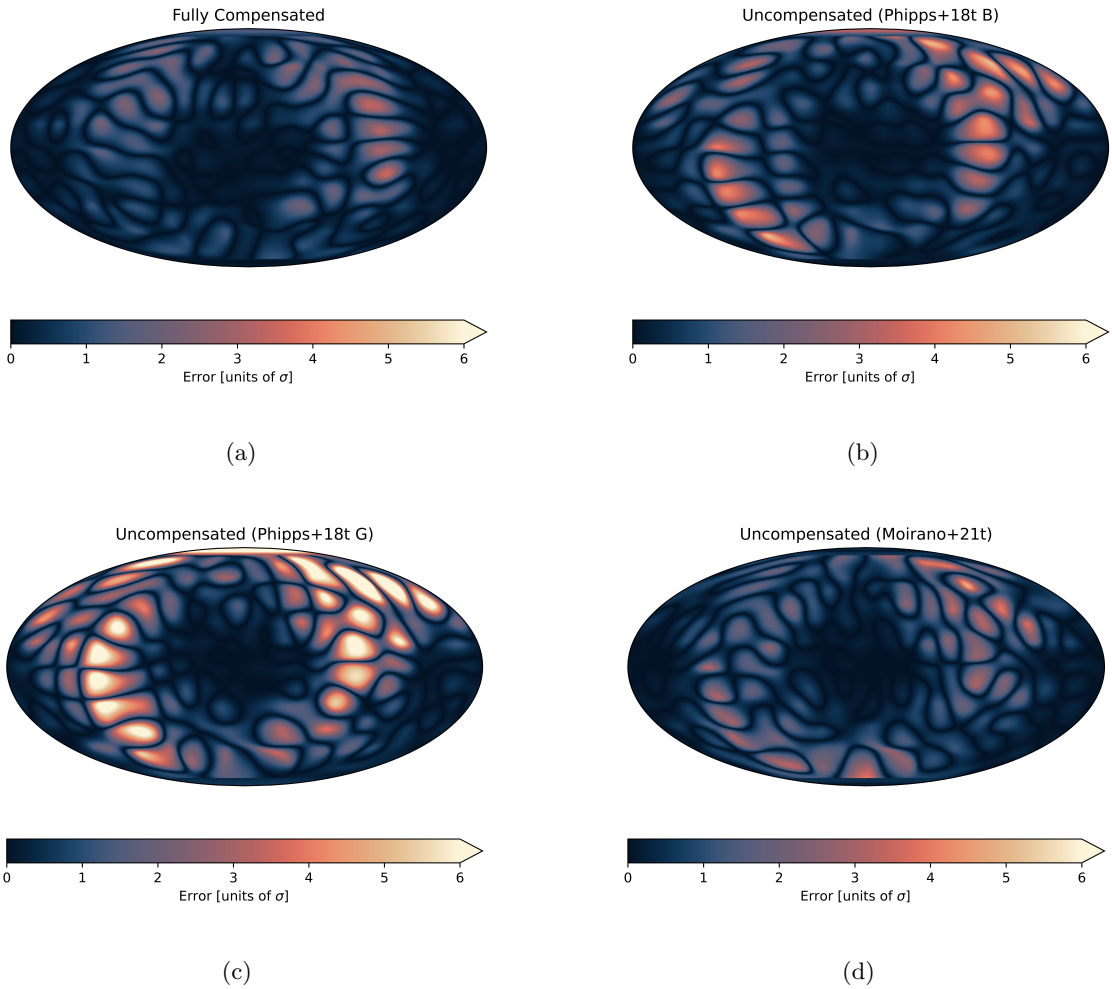

Figure 9: Spatial expansion of the gravity anomaly error, after normalization by the uncertainty. The four maps show the estimation error (in units of formal uncertainty σ) for the same cases discussed in Figure 8

Table 1: Estimation error (in units of σ) for the different tested cases. We report also the actual value of the formal uncertainty for comparison. Note that the latter are generally smaller than what reported by Mazarico et al. (2023), since here we have applied no multiplicative margin factor. Note also that here we adopt the hydrostatic equilibrium assumption, and thus compute the MOIF through the Radau-Darwin formula (as in Mazarico et al. (2023), Equation 4)

		Uncompensated (Sec 4.1)			Partially Compensated (Sec. 4.2)		
	Fully Compensated	Phipps+18t B	Phipps+18t G	Moirano+21t	Phipps+18t G	Moirano+21t	Sigma
GM	1.4	2.8	4.4	0.6	0.5	3.8	0.0005 km^3/s^2
k_2	0.5	0.15	0.9	0.9	1.2	1.1	0.007
MOIF	0.01	2.3	0.7	3.0	2.2	0.8	0.0002
J_2/C_{22}	0.007	3.7	3.5	3.5	1.0	0.7	0.002

1 show the different behavior of the two solutions. Most notably when calibrating with the Moirano+21t model, a large error on the GM is observed. Generally speaking, the partial calibration leads to reduced errors with respect to the uncalibrated case. The magnitude of the errors strongly depends on whether the underlying structure of the IPT

is well understood. Partially calibrating the signal with a model that well captures the structure of the IPT results in lower errors, almost at the acceptable level (3σ). Using instead a model whose IPT location and structure is different than the real one, still leads to large unrecovered estimation errors.

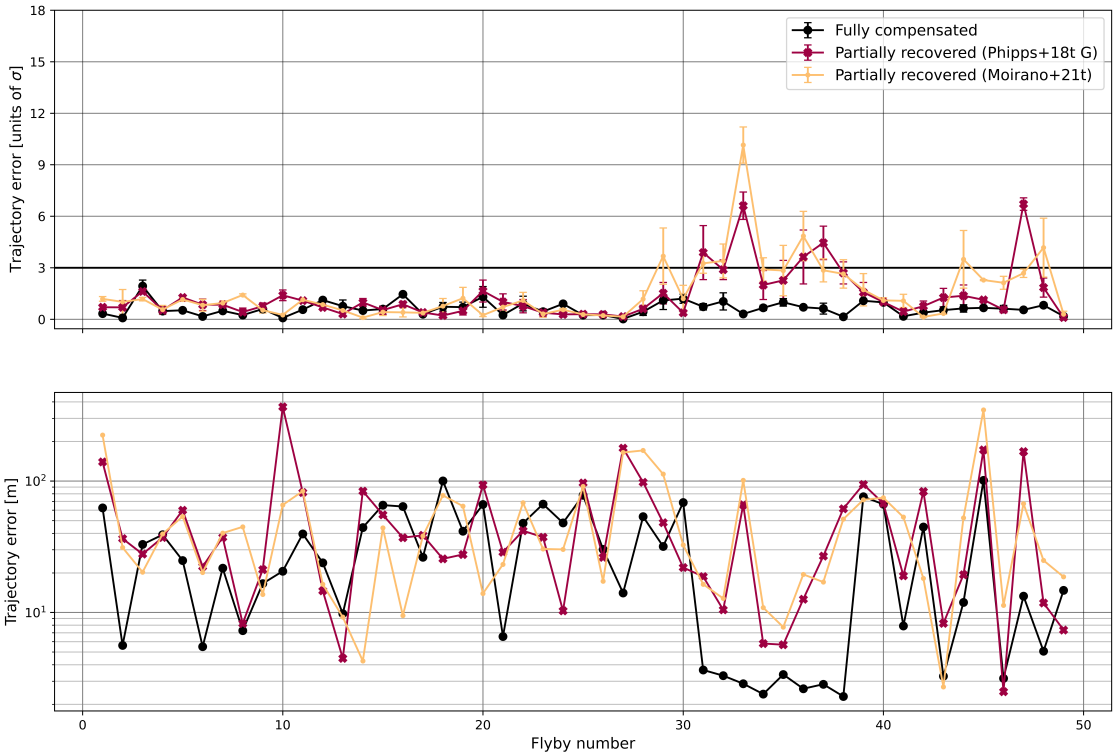

Figure 10: Trajectory error for each flyby. Both plots show the RMS trajectory error for different cases. The top panel reports the trajectory error normalized by the trajectory uncertainty (indicated by σ) together with its standard deviation (error bars), while the bottom plot shows the absolute value. The black lines show the error when the IPT perturbation is fully calibrated (same as in Figure 7). The red and yellow lines are obtained by calibrating the perturbations with the Phipps+18t G and Moirano+21t model, respectively. The trajectory errors are worse when the compensation is given by the Moirano+21t model because this latter is structurally different from the model used as ground truth (Phipps+18t B). The horizontal black line in the top panel highlights the 3σ level.

4.3. *IPT model intrinsic uncertainty*

We can already conclude that updated models of the IPT will be needed for fully exploiting the scientific potential of the G/RS investigation onboard Europa Clipper. To this aim additional ground based observations and future measurements enabled by ESA's JUICE plasma investigation (Grasset et al. 2013) or even the by-products of the plasma calibrations of its gravity and radioscience experiment (3GM, e.g., Di Stefano et al. 2022) will be invaluable to update the available IPT models. Given the very different trajectory of JUICE compared to Juno, we can expect it to sample different regions of the IPT and provide a more comprehensive view of its structure, more suited for the use in the Europa Clipper case. Even in this case, though, there will be inherent uncertainties on the model parameters. We want here to quantify the effect of model uncertainty on the trajectory and gravity reconstruction. To this aim we leverage the Moirano et al. (2021) model which naturally embeds temporal and longitudinal variabilities, and provides confidence bounds on the model parameters. In this case we will assume that the *true* behavior of the IPT is described by the Moirano+21t model using the central value of the model parameters, as published in the original

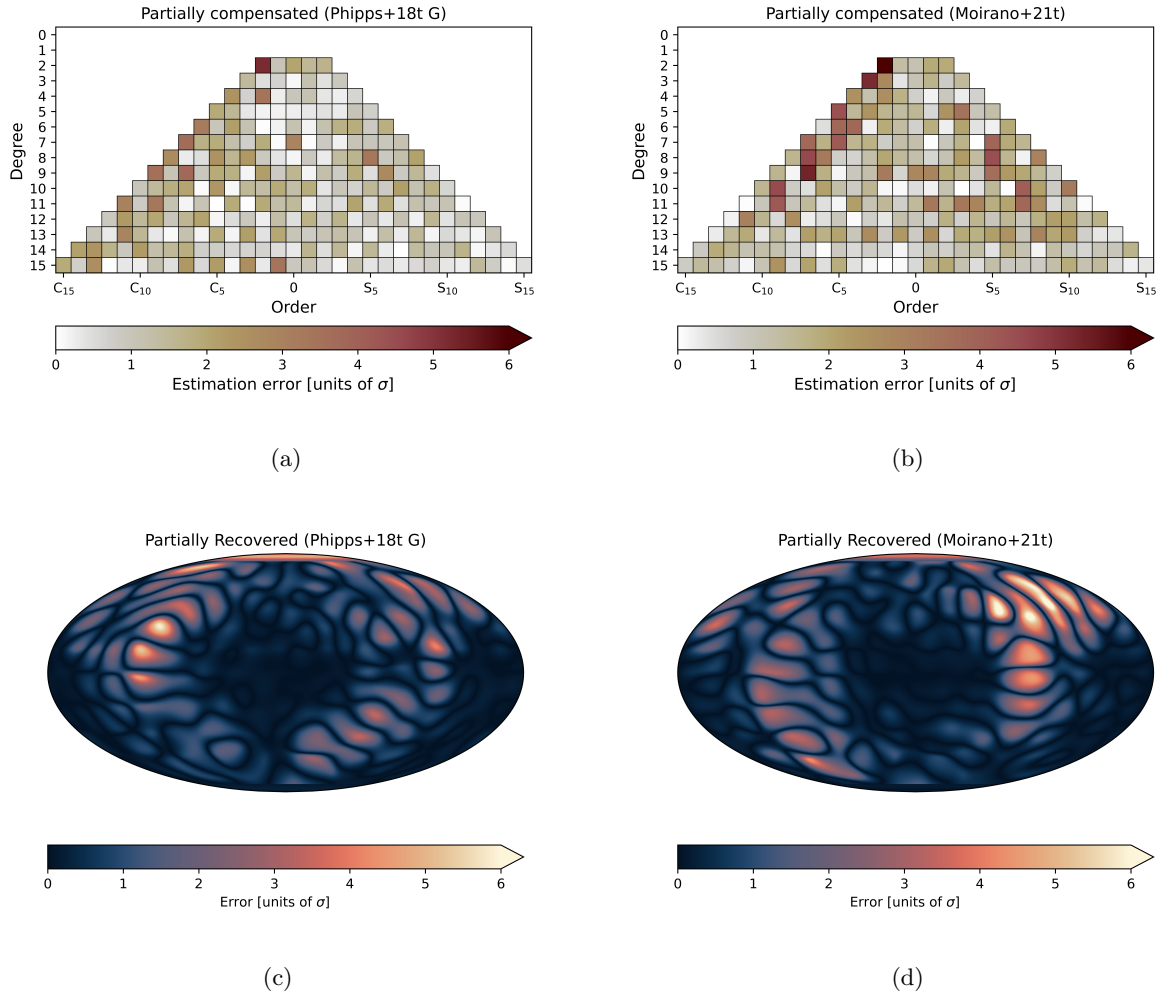

Figure 11: Gravity field spherical harmonics coefficients reconstruction error normalized by their formal uncertainty (σ) (See Figure 8).

manuscript, and compute the calibrations with different *realizations* of the model. To get a statistically relevant view of the expected outcome of such an approach we run multiple cases. In each case we compute the calibrations from the Moirano+21t model, perturbing the model parameters within their confidence bounds. We ran 20 cases where the model parameters have been perturbed at the 1σ level, 20 at 2σ, and 20 at 3σ. This means that the model parameters are drawn from a normal distribution with its mean equal to the parameter central value estimated in Moirano et al. (2021) and its standard deviation set to 1, 2, and 3 times the estimated uncertainty.

The overall calibration performance is highly ameliorated with respect to the partial calibration cases investigated above (Sec. 4.2). The trajectory reconstruction error, shown in Figure 12, is more consistent with the formal uncertainty, and only a few extreme cases show an error larger than three times the formal uncertainty. Namely this happens when the IPT perturbation is very strong and the model parameters are unknown at the three sigma level. The gravity field reconstruction (Figure 13) is better behaved as well, with minimal differences between the three cases investigated here (we report only the gravity field estimation error in the 3σ perturbation case, as the other two are very similar). The estimation error of the key geophysical parameters that we track here (the ones in Table 1) is strongly reduced, with all parameters showing an RMS estimation error below the 3σ level, with the GM being the most sensitive to the IPT perturbation, as discussed above, reaching an RMS error of 2 (in units of sigma) when the model is perturbed by 3σ. More details on the estimation error for these solutions can be found in Appendix E.

4.4. *Effect on Europa's ephemerides*

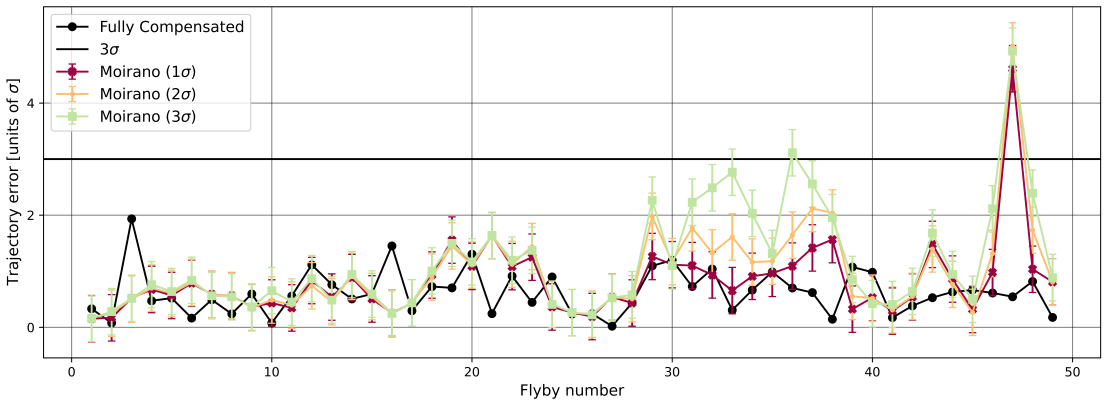

Figure 12: Trajectory reconstruction error due to model parameters uncertainty. For the three investigated cases (see text Section 4.3) we report the mean error and the standard deviation spread around the mean. These have been obtained by running 20 OD solutions for each investigated case $(1\sigma, 2\sigma, 3\sigma)$.

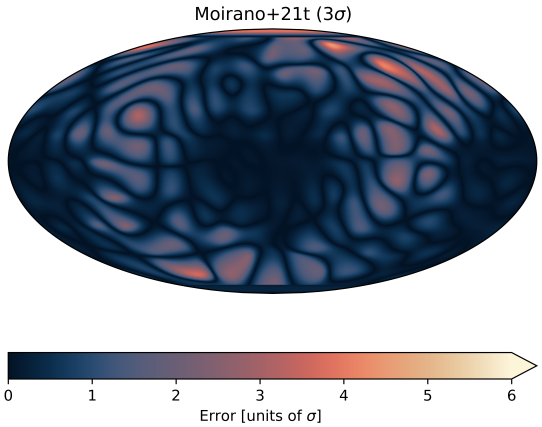

Figure 13: Gravity anomaly reconstruction error normalized by the formal uncertainty. This is the average reconstruction error when calibrating the tracking data with the Moirano model perturbed at the 3σ level. The 1σ and 2σ results are similar and not reported here.

Another important product of the G/RS investigation will consist in the estimation of the trajectory of Europa (also known as its ephemerides). This is done using the very same POD technique, analyzing not only the data at the closest approach ($\pm$ 2 hours as it's done for the gravity field estimation) but also the tracking passes extending 24 hours before and after the closest approach. Previous work has thoroughly assessed the capabilities of Europa Clipper to constrain Europa's orbit and its implication for deepening our dynamical understanding of the Jupiter system (Magnanini et al. 2024). Here we focus on the effect of the IPT on the ephemerides estimation performance. We have run the same simulations as in Magnanini et al. (2024), using the same IPT assessment approach of the previous sections. For an easier interpretation of the results we define the RTN (radial-transverse-normal) reference frame: centered on Europa, with the R axis directed towards Jupiter, the N axis parallel to Europa's orbital angular momentum and the T axis closing the triad. As it can be seen in Table 2, the expected errors due to the IPT is significant in the transverse direction, reaching up to 10 sigma in the uncalibrated case for all models considered. In the radial and normal components, the effect is limited to 1 standard deviation of the formal uncertainties, even in the uncalibrated scenario. However, in the partially calibrated case the errors in transverse decrease, becoming less than 3 standard deviations. In this work we do not address the estimation of Jupiter's tidal dissipation (that is directly

Table 2: Estimation error (in units of σ) for Europa's position with respect Jupiter Barycenter for the different tested cases, in the radial, transverse, and normal directions. For comparison, in the last column we report also the actual value of the formal uncertainty.

Direction	Maximum Error Uncompensated	Maximum Error Partially Compensated	Sigma
Radial	1.1	1.0	1-2 m
Transverse	10	3.0	2-10 m
Normal	0.8	0.5	30-50 m

determined from the ephemerides), since it requires further data from JUICE to obtain a statistically significant estimation (Magnanini et al. 2024). On the other hand, the estimation of Europa's orbital dissipation is dominated by the Europa Clipper data. In this case, the IPT can induce an estimation error of up to 2 standard deviations in the uncalibrated case, compared to only around 1 standard deviation in the calibrated case. Therefore, no substantial degradation in the estimation of Europa's dissipation is expected.

5. DISCUSSION

Our simulation results clearly highlight the necessity of updated models of the Io Plasma Torus electron density. Work in the next years, ahead of the arrival of Europa Clipper in the Jupiter system, could revise the underlying mathematical structure of the currently available semi-empirical models (*i.e.,* Moirano et al. (2021); Phipps et al. (2018, 2021)) to make them more applicable to Europa Clipper. Importantly, we have shown that the updates to earlier physics-based models in recent years, have applied simplifying assumptions that are well-suited for the Juno orbital geometry, but not applicable to other such as Europa Clipper and JUICE . In this work we have smoothed the electron densities at the boundaries between the model regions in the available empirical models, reducing the artifacts imparted by their non continuous differentiability when applied to the Europa Clipper geometry. Our choice of a smoothing function (see Appendix B) was, however, arbitrary and not based on any data or physical consideration. Future efforts are needed to ensure the continuous differentiability of $n_e(x, y, z)$ not only in the Juno geometry, but in all likely geometries of probes flying in the Jupiter system. This is an effort that could be undertaken with the currently available data (Voyager, Galileo, Juno), and would benefit from future observation campaigns.

Juno, is now in its extended mission, whereby the spacecraft will pass directly through regions of the Io Torus. During these periods Juno may be able to make in-situ measurements (e.g., Sulaiman et al. (2024)) in addition to radio occultations, providing valuable data to constrain future models.

ESA's JUICE mission, thanks to its multi-frequency radio link, could play an important role in providing high-quality geometrically-complementary information and reduce the current ambiguities in the Juno observations. Moreover future efforts could also include ground-based (e.g., Nerney et al. (2024)) or space-based observations, such as Hubble (as suggested by Schok et al. (2023)). Europa Clipper itself could provide useful calibration data, either using its onboard ultraviolet spectrograph (Europa-UVS, Davis et al. (2022)) or even carefully-planned radio-tracking passes. During the first half of the tour, the flybys will occur in a geometry that is not perturbed by the IPT (as discussed in Sec 4). But during that period, the apoapses of the orbits will be heavily perturbed by the IPT. The dynamics of the spacecraft near apoapsis is relatively *quiet*, *i.e.,* forces acting on the spacecraft change over long time scales. This means that the trajectory can be propagated more easily than during the flybys. Thus, one could expect the majority of the residual Doppler signal to be due to the IPT itself, allowing to directly extract the TEC of the regions crossed by the radio beam, and subsequently assimilate these observations into new empirical models of n_e.

Besides ameliorating the geometry and continuity of currently-available empirical models, we have shown that another important task for the coming years will be reducing the spread between them. Although current models describe the IPT perturbation effectively, in individual Juno flybys, the intrinsic differences between them lead to substantially different results, when applied across the entire span of the Europa Clipper mission, as detailed in Section 4.2. Thus, an effort towards unifying different models would be beneficial, such that the number of plausible applicable different models could be reduced. The inclusion of additional observational constraints (as discussed above) will also play a fundamental role in reducing the intrinsic uncertainty of model parameters. We have shown that current uncertainty

bounds can still lead to significant errors, especially for the estimate of the GM of Europa. Thus, a reduction of the model parameter uncertainties is important. This effort could be undertaken specifically for the case of Europa Clipper, by gauging the sensitivity of the G/RS experiment to each model parameter, thereby restricting the number of parameters of interest to be refined. If such an effort highlights that only a subset of parameters drive the solution, specific observation campaigns could be planned to investigate that subset of parameters. Alternatively, or additionally, one could re-parameterize the empirical models to depend solely on the most important parameters, simplifying the computation of the calibrations and the interpretation of the results.

Another direction that could be worth exploring consists in abandoning the semi-empirical descriptions of the IPT and resorting to physics based modeling. While models within this class have the advantage of encompassing more complex physical phenomena, they have the clear disadvantage of a substantially higher computational burden, making their integration in the OD process complicated. The first of such models, based upon in-situ Voyager data, was presented in Bagenal (1994b) and has been used for Juno (Yang et al. 2022). However, it was not used to calibrate the tracking data, since a multi-frequency link available. Newer models of the Io Plasma Torus, such as those presented by Hinton et al. (2017) and Hinton (2018) may also prove useful. One limitation of using a numerically-evaluated model is that it cannot be directly adjusted (because of the computational cost). One possible solution then, is to evaluate the expected frequency shift and estimate a scale factor and timing offset to compensate for local variations in the torus from either time-variability or longitude-variability and eventually feed these values back in the model to allow for its update.

6. CONCLUSION

In this work we have quantified the detrimental effect that the IPT might have on the Europa Clipper G/RS experiment, if not properly calibrated. While the retrieval of the tidal response of Europa, the only science requirement of G/RS, is robust to the radiometric perturbations induced by the Jovian plasma environment, the observation of other key geophysical quantities, and the reconstruction of the probe trajectory, might be severely affected. We have reviewed the main physical models describing the IPT and shown that these are not directly applicable to Jupiter system tour missions such as Europa Clipper and JUICE, and additional work will be needed in the coming years. We have assessed the effectiveness of model-based calibration techniques, showing that these can have a substantial effect in reducing the error on the estimated quantities, provided that the differences between currently available models of the IPT are understood and resolved. We hope that the outcome of this work will serve as a motivation for future investigations aiming to improve the currently available IPT models by including additional already available data and pushing for additional observations possible in the present and in the coming years.

ACKNOWLEDGEMENTS

The authors would like to thank P. Phipps (University of Maryland Baltimore County) for fruitful discussions and clarifications. Work by G.C. was supported by NASA under award No. 80GSFC24M0006. Part of this research was carried out at the Jet Propulsion Laboratory, California Institute of Technology, under a contract with the National Aeronautics and Space Administration (80NM0018D0004). A.M., M.Z., L.G.C, and P.T. acknowledge financial support from the Italian Space Agency through the Agreement 2021-13- HH.1-2023.

APPENDIX

A. BASIC THEORY OF ORBIT DETERMINATION

Here we give a brief overview of the POD process and equations. We discuss how the solution and associated uncertainties are obtained. The purpose of this appendix is to provide the interested reader a sense of how the uncertainty and estimation error (two quantities extensively used in this work to gauge the impact of the IPT) are computed. The reader is referred to the specialized POD literature for more details (*e.g.,* Tapley et al. (2004); Moyer (2003); Milani & Gronchi (2009); Montenbruck & Gill (2000), see also Cascioli et al. (2023, 2020); Cascioli & Genova (2021) for more detailed applications using the same nomenclature).

The POD process aims to find the combination of the spacecraft dynamical model parameters that allow to best fit the tracking data. Defining $\mathbf{X}_0$ as the dynamical model state vector at a given time ($t = t_0$), the POD solution will aim to find the value of $\mathbf{X}_0$ that produces an estimated trajectory as close as possible as the true one. It can be easily understood that the equations governing the spacecraft motion are highly non-linear. A commonly used approach consists in linearizing the dynamical model. As such, the problem is formulated in terms of *deviations*, i.e., differences with respect to the truth. For example $\mathbf{x}_0 = \mathbf{X}_0 - \mathbf{X}_0^*$ is the *state deviation vector*: the difference between the state vector ($\mathbf{X}_0$) and the *true* state vector ($\mathbf{X}_0^*$). The minimum variance least-squares estimate of the state deviation vector, $\hat{\mathbf{x}}_0$ is:

$$\hat{\mathbf{x_0}} = \left(H^T R^{-1} H + \bar{P}_0^{-1}\right)^{-1} \left(H^T R^{-1} \mathbf{y} + \bar{P}_0^{-1} \bar{\mathbf{x}}_0\right) \tag{A1}$$

where $\mathbf{y}$ is the observations deviation vector (the difference between the *observed* observables and the *computed* observables, *i.e.,* the residuals), H is the mapping matrix containing the partial derivatives of the observations with respect to the state vector components at the reference time, $\bar{P}_0$ is the apriori covariance matrix of the state vector components, and R is the observation noise covariance matrix. A fundamental quantity associated to the estimated state vector $\hat{\mathbf{x}}_0$ is its associated variance-covariance matrix P_0. P_0 contains the covariance of the state vector components (at time t_0) and it is influenced by the quality of the data, the geometry of the problem, and the apriori assumptions:

$$P_0 = \left(H^T R^{-1} H^+ \bar{P}_0^{-1}\right)^{-1} \tag{A2}$$

The covariance matrix P can be mapped at any given time t through:

$$P(t) = \Phi(t, t_0) P_0 \Phi^T(t, t_0) \tag{A3}$$

where $\Phi(t, t_0)$ is the state transition matrix, *i.e.,* the matrix mapping the state vector between times t and t_0:

$$\mathbf{x}_t = \Phi(t, t_0) \mathbf{x}_0 \tag{A4}$$

In this work we make use of two main quantities: the estimation error and the formal uncertainty. The estimation error is the difference between the *estimated* state vector $\hat{\mathbf{X}}$ and the *true* state vector $\mathbf{X}$ (that we know because we are in a simulation setting). The formal uncertainty on the state vector components is no other than the square root of the diagonal of P.

In the main text we often use the ratio between the true error and the formal uncertainty. This is a useful quantity for understanding wether the OD solution is valid. From a statistical point of view, the OD solution is guaranteed to be unbiased within bounds defined by the formal uncertainty (the posterior distribution of the estimated parameters is Gaussian). When unmodeled perturbations are introduced (*i.e.,* systematic errors), however, the actual bias of the solution might be outside the bounds predicted by the formal uncertainty. What motivates this manuscript is the necessity to understand what would be the effect of the IPT on the validity of the OD solution. In the majority of cases, reported in the main text, the observation residuals -even in the presence of and unmodeled IPT perturbation- are well comparable to white noise, thus suggesting an unbiased solution. A simulation setting, where the *truth* is known, allows to precisely quantify the bias in the solution, by comparing the estimation error to the formal uncertainty. When the estimation error is substantially larger than the formal uncertainty the solution is biased.

B. REMOVING DISCONTINUITIES FROM THE MODELS

We use a logistic taper defined by:

$$T(r) = \frac{1}{1 + e^{-k(r - r_0)}} \tag{B5}$$

where r is the radial planar coordinate in the Io centrifugal equator frame, k defines the steepness of $T(r)$ and r_0 is the center-point of the taper. $T(r)$ is used as a connection between different segments of the electron density models. As an example here below we report the Phipps et al. (2018) model (the very same procedure applies to the models from Moirano et al. (2021), which we do not report here for brevity):

$$\begin{aligned} N(r < 6.1R_J, z) &= N_1 e^{-\frac{(r-C_1)^2}{W_1^2}} e^{-\frac{z^2}{H_1^2}} + N_2 e^{-\frac{(r-C_2)^2}{W_2^2}} e^{-\frac{z^2}{H_2^2}} + N_3 e^{-\frac{(r-C_3)^2}{W_3^2}} e^{-\frac{z^2}{H_3^2}} \\ N(r > 6.R_J, z) &= N_4 e^{-\frac{(r-C_4)^2}{W_4^2}} e^{-\frac{z^2}{H_4^2}} \end{aligned} \tag{B6}$$

the modified model becomes:

$$\begin{aligned} N(r < 6.1R_J, z) &= N_1 e^{-\frac{(r-C_1)^2}{W_1^2}} e^{-\frac{z^2}{H_1^2}} + N_2 e^{-\frac{(r-C_2)^2}{W_2^2}} e^{-\frac{z^2}{H_2^2}} + (1 - T(r)) N_3 e^{-\frac{(r-C_3)^2}{W_3^2}} e^{-\frac{z^2}{H_3^2}} \\ N(r > 6.R_J, z) &= T(r) N_4 e^{-\frac{(r-C_4)^2}{W_4^2}} e^{-\frac{z^2}{H_4^2}} \end{aligned} \tag{B7}$$

For the Phipps model we adopt $r_0 = 6.05R_J$, $k = 1.1 \times 10^{-3}$ and for the Moirano models we adopt $r_0 = 5.35R_J$, $k = 6 \times 10^{-4}$.

C. GRAVITY ERROR MAPS

Figure 14 reports the formal uncertainty of the gravity anomaly that will be retrieved by Europa Clipper. Figure 15 reports the estimation error in absolute value for the same cases discussed in Figure 9

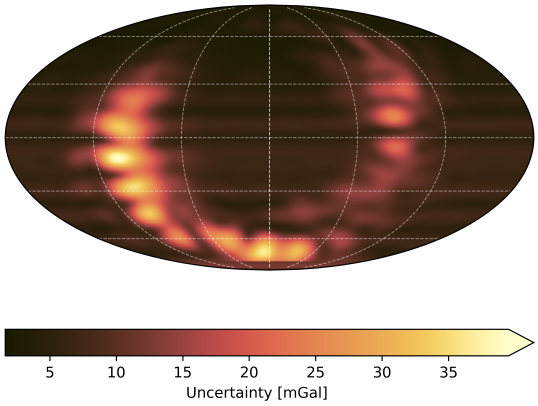

Figure 14: Gravity anomaly uncertainty

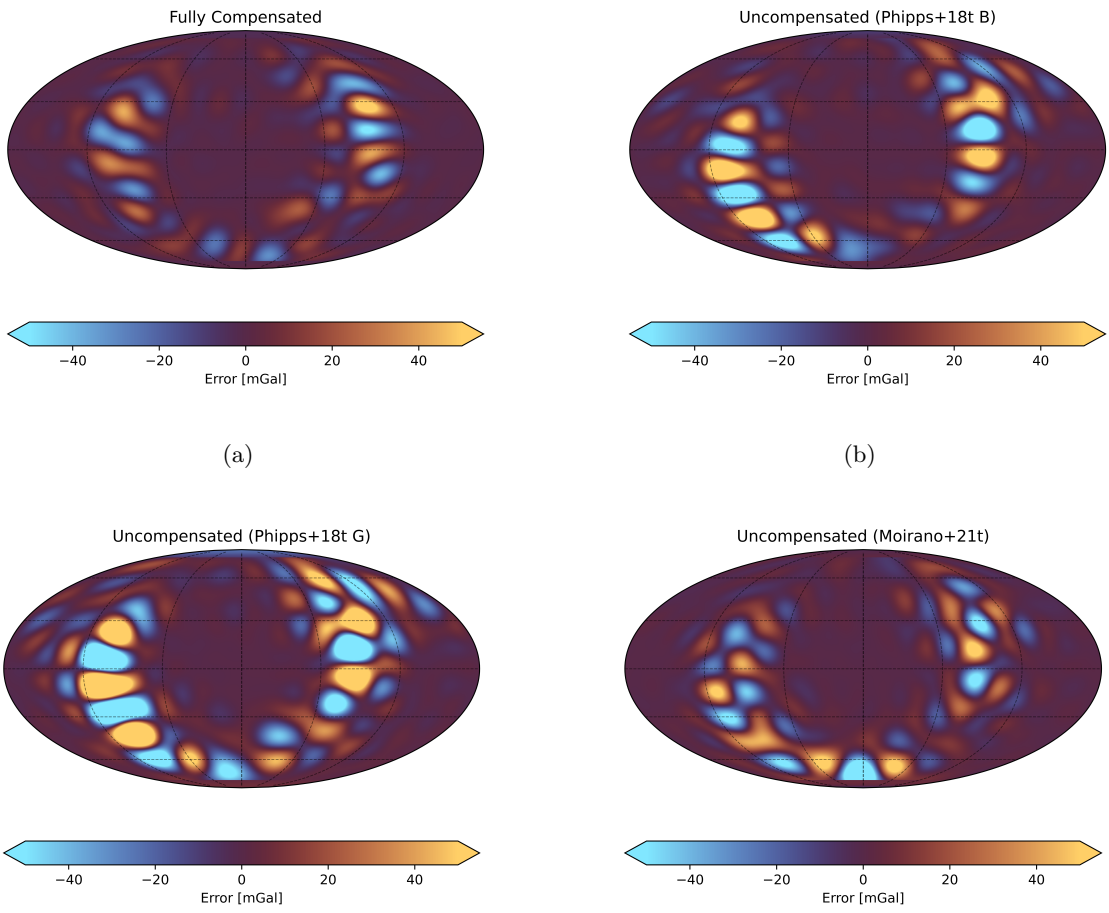

Figure 15: Gravity anomaly error.

D. GROUND TRACKS

Here, for better understanding how the different models influence data collection, we report the ground tracks of Europa clipper, color-coded by the IPT perturbation. The size of the lines for every ground track is dependent on the distance between the probe and the surface of Europa. The largest portion of a ground track line is the closest approach.

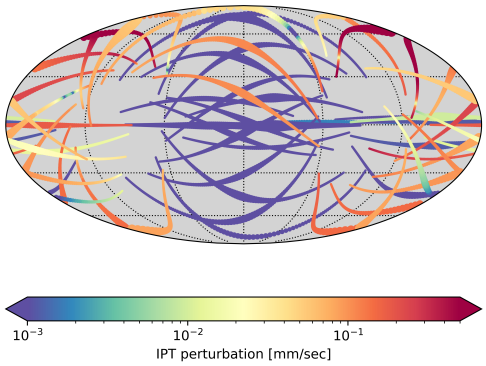

(a) Phipps+18t B

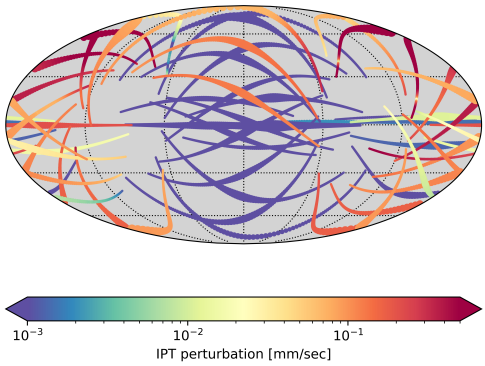

(b) Phipps+18t G

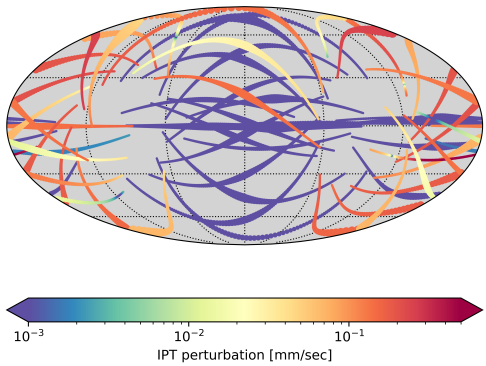

(c) Moirano+21t

Figure 16: Ground tracks of the 49 Europa Clipper flybys, color-coded by the IPT doppler perturbation magnitude. The tracks are shown in a Mollweide equal area projection centered at 180° longitude.

E. RECONSTRUCTION ERRORS DUE TO MODEL UNCERTAINTY

Here below we report statistics on the estimation error (in units of sigma) due to the model parameters uncertainty (see section 4.3). For each parameter and each investigated case, we report the RMS error, the minimum and the maximum

Table 3: Estimation error due to model uncertainty. Here we report for each tracked parameter the RMS, minimum and maximum estimation error (in units of sigma) for the three investigated cases (see text in Section 4.3)

	Moirano+21t 1σ			Moirano+21t 2σ			Moirano+21t 3σ			
	RMS	Min	Max	RMS	Min	Max	RMS	Min	Max	Sigma
GM	0.6	0.02	1.7	2.0	0.4	4.9	2.1	0.1	4.9	0.0005 km^3/s^2
k_2	0.2	0.001	0.4	0.4	0.04	0.7	0.4	0.01	0.7	0.007
MOIF	0.4	0.002	1.01	0.5	0.04	1.3	1.1	0.08	2.1	0.0002
J_2/C_{22}	0.6	0.03	1.0	0.7	0.04	1.8	1.3	0.003	2.5	0.002

REFERENCES

Asmar, S. W., Bolton, S. J., Buccino, D. R., et al. 2017, Space Science Reviews, 213, 205, doi: 10.1007/s11214-017-0428-7

Bagenal, F. 1994a, Journal of Geophysical Research: Space Physics, 99, 11043, doi: 10.1029/93JA02908

—. 1994b, Journal of Geophysical Research: Space Physics, 99, 11043, doi: 10.1029/93JA02908

Bagenal, F., Crary, F. J., Stewart, A. I. F., et al. 1997, Geophysical Research Letters, 24, 2119, doi: 10.1029/97GL01254

Bagenal, F., & Delamere, P. A. 2011, Journal of Geophysical Research: Space Physics, 116, doi: 10.1029/2010JA016294

Bagenal, F., Dougherty, L., Bodisch, K., Richardson, J., & Belcher, J. 2017, Journal of Geophysical Research: Space Physics, 122, 8241, doi: https://doi.org/10.1002/2016JA023797

Bagenal, F., & Sullivan, J. D. 1981, Journal of Geophysical Research: Space Physics, 86, 8447, doi: https://doi.org/10.1029/JA086iA10p08447

Bagenal, F., Sullivan, J. D., & Siscoe, G. L. 1980, Geophysical Research Letters, 7, 41, doi: 10.1029/GL007i001p00041

Bertotti, B., Comoretto, G., & Iess, L. 1993, A&A, 269, 608

Bertotti, B., Comoretto, G., & Iess, L. 1993, Astronomy and Astrophysics, 269, 608

Bertotti, B., Iess, L., & Tortora, P. 2003, Nature, 425, 374, doi: 10.1038/nature01997

Bird, M., Asmar, S., Edenhofer, P., et al. 1993, Planetary and Space Science, 41, 999, doi: 10.1016/0032-0633(93)90104-A

Bird, M. K., Asmar, S. W., Brenkle, J. P., et al. 1992, Science, 257, 1531, doi: 10.1126/science.257.5076.1531

Bridge, H. S., Belcher, J. W., Lazarus, A. J., et al. 1979, Science, 204, 987, doi: 10.1126/science.204.4396.987

Cappuccio, P., Ruscio, A. D., Iess, L., & Mariani, M. J. 2020, doi: 10.2514/6.2020-1095

Cascioli, G., Durante, D., Mazarico, E., et al. 2023, Journal of Spacecraft and Rockets, 60, 366

Cascioli, G., & Genova, A. 2021, Journal of Spacecraft and Rockets, 58, 581

Cascioli, G., Mazarico, E., Dombard, A., & Nimmo, F. 2024, The Planetary Science Journal, 5, 45

Cascioli, G., Petricca, F., & Genova, A. 2020, Acta Astronautica, 177, 103

Davis, M. W., Retherford, K. D., Molyneux, P. M., et al. 2022, in Space Telescopes and Instrumentation 2022: Ultraviolet to Gamma Ray, ed. J.-W. A. Den Herder, K. Nakazawa, & S. Nikzad (Montréal, Canada: SPIE), 120, doi: 10.1117/12.2630530

Di Stefano, I., Cappuccio, P., Di Benedetto, M., & Iess, L. 2022, Advances in Space Research, 70, 854, doi: 10.1016/j.asr.2022.05.005

Durante, D., Parisi, M., Serra, D., et al. 2020, Geophysical Research Letters, 47, doi: 10.1029/2019GL086572

Eshleman, V. R., Tyler, G. L., Wood, G. E., et al. 1979, Science, 206, 959, doi: 10.1126/science.206.4421.959

Gomez Casajus, L., Zannoni, M., Modenini, D., et al. 2021, Icarus, 358, 114187, doi: 10.1016/j.icarus.2020.114187

Grasset, O., Dougherty, M., Coustenis, A., et al. 2013, Planetary and Space Science, 78, 1, doi: 10.1016/j.pss.2012.12.002

Hinton, P. 2018, PhD thesis. https://scholar.colorado.edu/concern/undergraduate_honors_theses/jh343s81x

Hinton, P. C., Bagenal, F., & Bodisch, K. M. 2017, 2017, SM33C. https://ui.adsabs.harvard.edu/abs/2017AGUFMSM33C2669H

Kupo, I., Mekler, Y., & Eviatar, A. 1976, The Astrophysical Journal, 205, L51, doi: 10.1086/182088

Magnanini, A., Zannoni, M., Casajus, L. G., et al. 2024, Astronomy & Astrophysics, 687, A132, doi: 10.1051/0004-6361/202347616

Mazarico, E., Buccino, D., Castillo-Rogez, J., et al. 2023, Space Science Reviews, 219, 30, doi: 10.1007/s11214-023-00972-0

Milani, A., & Gronchi, G. 2009, Theory of Orbit Determination (Cambridge University Press), doi: 10.1017/CBO9781139175371

Moirano, A., Gomez Casajus, L., Zannoni, M., Durante, D., & Tortora, P. 2021, Journal of Geophysical Research: Space Physics, 126, e2021JA029190, doi: 10.1029/2021JA029190

Montenbruck, O., & Gill, E. 2000, in Satellite Orbits (Berlin, Heidelberg: Springer Berlin Heidelberg), 257–291, doi: 10.1007/978-3-642-58351-3_8

Moyer, T. D. 2003, Formulation for Observed and Computed Values of Deep Space Network Data Types for Navigation (John Wiley & Sons, Inc.), doi: 10.1002/0471728470

Nerney, E. G., Bagenal, F., & Schmidt, C. A. 2024, Simulations of Optical Emissions in Io's Plasma Torus, doi: 10.22541/essoar.172526827.77237465/v1

Pappalardo, R. T., Buratti, B. J., Korth, H., et al. 2024, Space Science Reviews, 220, 40, doi: 10.1007/s11214-024-01070-5

Peale, S. J., Cassen, P., & Reynolds, R. T. 1979, Science, 203, 892, doi: 10.1126/science.203.4383.892

Phipps, P. H., & Withers, P. 2017, Journal of Geophysical Research: Space Physics, 122, 1731, doi: 10.1002/2016JA023447

Phipps, P. H., Withers, P., Buccino, D. R., & Yang, Y. 2018, Journal of Geophysical Research: Space Physics, 123, 6207, doi: 10.1029/2017JA025113

Phipps, P. H., Withers, P., Buccino, D. R., Yang, Y., & Parisi, M. 2019, Journal of Geophysical Research: Space Physics, 124, 5200, doi: 10.1029/2018JA026297

—. 2021, Journal of Geophysical Research: Space Physics, 126, doi: 10.1029/2020JA028710

Schok, A. A., Delamere, P. A., Mino, B., et al. 2023, Journal of Geophysical Research: Planets, 128, e2022JE007637, doi: 10.1029/2022JE007637

Sulaiman, A. H., Kurth, W. S., Connerney, J. E. P., et al. 2024, Geophysical Research Letters, 51, e2024GL110206, doi: 10.1029/2024GL110206

Tapley, B. D., Schutz, B. E., & Born, G. H. 2004, Statistical Orbit Determination (Elsevier), doi: 10.1016/B978-0-12-683630-1.X5019-X

Yang, Y.-M., Buccino, D., Parisi, M., et al. 2022. https://ui.adsabs.harvard.edu/abs/2022AGUFM.P41D..02Y